

# New activation cross section data on longer lived radio-nuclei produced in proton induced nuclear reaction on zirconium

F. Tárkányi<sup>a</sup>, F. Ditrói<sup>a,\*</sup>, S. Takács<sup>a</sup>, A. Hermanne<sup>b</sup>, M. Al-Abyad<sup>c</sup>, H. Yamazaki<sup>d</sup>, M. Baba<sup>d</sup>, M.A. Mohammadi<sup>d</sup>

<sup>a</sup>*Institute for Nuclear Research, Hungarian Academy of Sciences (ATOMKI), Debrecen, Hungary*

<sup>b</sup>*Cyclotron Laboratory, Vrije Universiteit Brussel (VUB), Brussels, Belgium*

<sup>c</sup>*Physics Department, Cyclotron Facility, Nuclear Research Centre, Atomic Energy Authority, Cairo 13759, Egypt*

<sup>d</sup>*Cyclotron and Radioisotope Center (CYRIC), Tohoku University, Sendai, Japan*

---

## Abstract

In the frame of a systematic study of charged particle production routes of medically relevant radionuclei, the excitation function for indirect production of  $^{178m}\text{Ta}$  through  $^{nat}\text{Hf}(\alpha, xn)^{178-178m}\text{Ta}$  nuclear reaction was measured for the first time up to 40 MeV. In parallel, the side reactions  $^{nat}\text{Hf}(\alpha, x)^{179,177,176,175}\text{W}$ ,  $^{183,182,178g,177,176,175}\text{Ta}$ ,  $^{179m,177m,175}\text{Hf}$  were also assessed. Stacked foil irradiation technique and  $\gamma$ -ray spectrometry were used. New experimental cross section data for the  $^{nat}\text{Ta}(d, xn)^{178}\text{W}$  reaction are also reported up to 40 MeV. The measured excitation functions are compared with the results of the ALICE-IPPE, and EMPIRE nuclear reaction model codes and with the TALYS 1.4 based data in the TENDL-2013 library. The thick target yields were deduced and compared with yields of other charged particle ((p,4n), (d,5n) and ( $^3\text{He},x$ )) production routes for  $^{178}\text{W}$ .

*Keywords:* proton activation, cross section measurement, yield calculation, Nb, Zr and Y radioisotopes

---

## 1. Introduction

Production cross sections of proton induced nuclear reactions on metals are important for many applications and for development of improved nuclear reaction theory. In most applications high intensity, low and high energy direct or secondary proton beams activate technological elements and produce highly active radio-products. After recognizing the importance of knowledge of production cross sections we concluded that a systematic coordinated experimental and theoretical study is necessary, and we started a set of experiments with a large scope. Our research in connection with the activation cross sections on zirconium is of importance and applies to different projects:

- Preparation of a nuclear database for production of  $^{90}\text{Nb}$ ,  $^{95}\text{Nb}$ ,  $^{89}\text{Zr}$ ,  $^{88}\text{Y}$  medical radioisotopes in the frame of IAEA Coordinated Research Project (Gul et al., 2001; IAEA, 2001, 2012-2016) using the  $^{90}\text{Zr}(p,n)^{90}\text{Nb}$ ,  $^{96}\text{Zr}(p,2n)^{95}\text{Nb}$ ,  $^{90}\text{Zr}(p,2n)^{89}\text{Nb}$ ,  $^{89}\text{Zr}$  and  $^{nat}\text{Zr}(p,x)^{88}\text{Zr} \rightarrow ^{88}\text{Y}$  production routes. We have also investigated alternative production

routes of these radio-products on yttrium (Uddin et al., 2007, 2005).

- Preparation of proton and deuteron activation cross section database for the Fusion Evaluated Nuclear Data Library (IAEA, 2004).
- Preparation of a database for the Thin Layer Activation (TLA) technique for wear measurement (IAEA-NDS, 2010) and every day practice of wear measurement of zirconium alloy samples.

We earlier reported on experimental activation cross section data on Zr targets for deuteron induced reactions up to 50 MeV (Tárkányi et al., 2004, 1985) and for proton reactions up to 17 MeV (Al-Abyad et al., 2012). During the compilation of the experimental data of proton induced activation a large disagreements in the database at higher energies were noted. Hence we decided to extend our investigations up to higher energies and to complete them by testing the prediction capabilities of the widely used TALYS model code.

---

\*Corresponding author: ditroi@atomki.hu

## 2. REVIEW OF EARLIER INVESTIGATIONS

### 2.1. Earlier experimental investigations

The earlier experimental investigations reported in the literature (also from our group) are compiled and shown in Table 1 that includes information on the used target, accelerator, beam monitoring, measurement of the activity, the measured data points, and the covered energy range. According to our tradition we have investigated the earlier experimental results and the theoretical results in detail before new experiments were designed and performed.

### 2.2. Earlier theoretical estimates and systematics

For estimation of production cross sections of proton induced reaction cross sections a few systematic theoretical calculations exist in the TENDL-2013 library (Koning et al., 2012) based on TALYS version 1.4 code (Koning et al., 2007), in the MENDL-2p library (Shubin et al., 1998) based on the ALICE-IPPE code (Dityuk et al., 1998), in the publication of Ren et al. up to 200 MeV (Ren et al., 2011) by using the MEND (Cai, 2006) code, and in the publication by Sadeghi et al. and Broeders et al. based on the ALICE/ASH code (Broeders and Konobeyev, 2007; Sadeghi et al., 2011). Nuclear reaction systematics, semi-empirical formulas are also used for the evaluation of reaction cross-section to supplement to the result of measurements and calculations by theoretical models (Tel et al., 2010).

## 3. Experimental techniques and data evaluation

### 3.1. Experiment

The excitation functions for the  $^{nat}\text{Zr}(p,x)$  reactions were measured at the cyclotrons of the Vrije Universiteit Brussel (VUB, Brussels, Belgium) and of Tohoku University (CYRIC, Sendai, Japan) using the stacked foil technique. The experimental method used was similar to the techniques used in our numerous earlier investigations of charged particle induced nuclear reactions for different applications. Two stacks were irradiated using the 36 MeV (VUB) and 70 MeV (CYRIC) incident proton energy respectively. In both experiments natural, high purity Zr foils (Goodfellow, 99.98%, thickness 98.42  $\mu\text{m}$  and 103  $\mu\text{m}$ ) were assembled together with target foils of other elements for separate investigations and with monitor and degrader foils. The target stack at VUB was composed of Ho (26.2  $\mu\text{m}$ ), Zr (98.42  $\mu\text{m}$ ), Al degraders (156.56  $\mu\text{m}$ ), Pb (15.74  $\mu\text{m}$ ) and Ti monitor (12  $\mu\text{m}$ ) foils, repeated 12 times. The stack composition at higher energy irradiation at CYRIC: Zr(103  $\mu\text{m}$ ),

Rh (12.3  $\mu\text{m}$ ), Al (520  $\mu\text{m}$ , degrader, and monitor), Mn(10  $\mu\text{m}$ ), Al (520  $\mu\text{m}$ , degrader, and monitor) and Ag (52  $\mu\text{m}$ ), repeated 19 times. The Ti and Al monitor foils were used for determination of beam intensity and energy by re-measuring the excitation function for the  $^{nat}\text{Ti}(p,x)^{48}\text{V}$  reaction at VUB and  $^{27}\text{Al}(p,x)^{22,24}\text{Na}$  reactions at CYRIC over the entire covered energy range. The target stacks were irradiated in a Faraday-cup like target holder. Irradiations took place at beam current of 160 nA for 60 min (VUB) and 24 nA for 30 min (CYRIC) respectively. The gamma activity of the majority of the produced radionuclides was measured with standard high purity Ge detectors coupled to acquisition/analysis software. No chemical separation was performed and the measurements were repeated several times up to several months after EOB. Due to large number of simultaneously irradiated targets and the limited detector capacity the first measurements of the induced activity started on both cases after relatively long cooling times ( VUB:1.5 day, CYRIC: 3 day after EOB).

### 3.2. Data processing

For most of the assessed radionuclides different independent  $\gamma$ -lines are available allowing an internal check of the consistency of the calculated activities. The decay and spectrometric characteristics were taken from the NUDAT2 data base (NuDat, 2014) and are summarized in Table 2. The cross sections were calculated from the well-known activation formula with measured activity, particle flux and number of target nuclei as input parameters. Some of the radionuclides formed are the result of cumulative processes as decay of metastable states or parent nuclides contribute to the production process. The exact physical situation for the individual studied nuclides will be discussed in the next sections. The particle flux was initially derived through total charge on target by the Faraday cup using a digital integrator. The incident beam energy was determined from the accelerator settings and the mean energy in each foil was calculated by polynomial approximation of Andersen and Ziegler (Andersen and Ziegler, 1977) or calculated with the help of the SRIM code (Ziegler, 2013). The beam energy and intensity parameters were corrected by taking into account the comparison of the excitation function of  $^{nat}\text{Ti}(p,x)^{48}\text{V}$  and  $^{27}\text{Al}(p,x)^{22,24}\text{Na}$  reactions, re-measured over the whole energy domain studied, with the recommended values in the updated version of IAEA-TECDOC 1211 (Tárkányi et al., 2001) (Fig. 1). The uncertainty of the incident energy on the first foil in both cases was around  $\pm 0.3$  MeV. Taking into account the cumulative effects of possible variation on incident energy and thickness of the

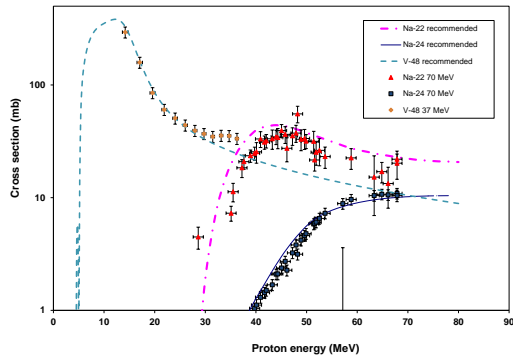


Figure 1: The re-measured cross sections of the used monitor reactions  $^{27}\text{Al}(p,x)^{22,24}\text{Na}$  and  $^{nat}\text{Ti}(p,x)^{48}\text{V}$  in comparison with the recommended data

different targets, the uncertainty on the median energy in the last foil was around  $\pm 1.2$  MeV. The uncertainty on each cross-section was estimated in the standard way (of-Weights-and Measures, 1993) by taking the square root of the sum in quadrature of all individual contributions, supposing equal sensitivities for the different parameters appearing in the formula. The following individual uncertainties are included in the determination of the peak areas including statistical errors (0.1-20 %): the number of target nuclei including non-uniformity (5 %), detector efficiency (5 %) and incident particle intensity (7 %). The total uncertainty of the cross-section values was evaluated to vary from 8 to 14 %, except for few cases where the statistical errors were high.

## 4. RESULTS

### 4.1. Cross sections

The numerical data of excitation functions of  $^{96}\text{Nb}$ ,  $^{95}\text{Nb}$ ,  $^{95g}\text{Nb}$ ,  $^{92m}\text{Nb}$ ,  $^{91m}\text{Nb}$ ,  $^{90}\text{Nb}$ ,  $^{95}\text{Zr}$ ,  $^{89}\text{Zr}$ ,  $^{88}\text{Zr}$ ,  $^{86}\text{Zr}$ ,  $^{88}\text{Y}$ ,  $^{87m}\text{Y}$ ,  $^{87g}\text{Y}$ ,  $^{86}\text{Y}$  are presented in Tables 3-5 and are shown in graphical form in Figures 2-15 for comparison with the earlier experimental data and with the theoretical values taken from the TENDL-2013 online library (Koning et al., 2012) calculated with the 1.4 version of TALYS (Koning et al., 2007). The contributing reactions and decay processes are presented in Table 2. The excitation functions are shortly discussed for each activation product separately.

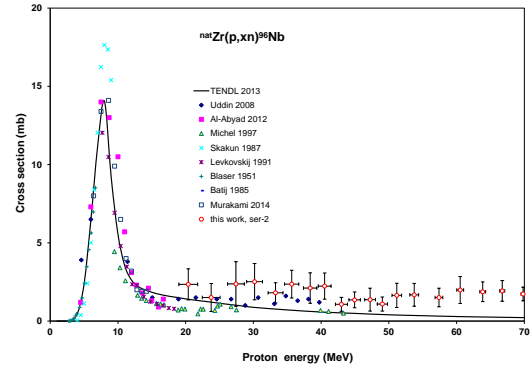


Figure 2: Excitation function of the  $^{nat}\text{Zr}(p,x)^{96}\text{Nb}$  reaction

#### 4.1.1. Cross sections of $^{96}\text{Nb}$

The radionuclide  $^{96}\text{Nb}$  ( $T_{1/2} = 23.35$  h) can only be produced via the  $^{96}\text{Zr}(p,n)$  reaction. Due to the experimental circumstances we could obtain data only from the high energy irradiation (Fig. 2) and the results have large uncertainties due to the low counting statistics. The agreement with the literature data and with the theory is acceptable.

#### 4.1.2. Cross sections of $^{95}\text{Nb}$

The radionuclide  $^{95}\text{Nb}$  has shorter-lived metastable state  $^{95}\text{Nb}$  ( $T_{1/2} = 86.64$  h) and a longer-lived ground state  $^{95g}\text{Nb}$  ( $T_{1/2} = 34.991$  d). The isomeric state decays to the ground state by 94.4% IT process. We obtained experimental data for  $^{95}\text{Nb}$  only from the low energy irradiation, the 235 keV  $\gamma$ -line of the metastable state could not be separated reliably in our spectra from the high energy experiment. Our results and the data of (Levkovskii, 1991) are in good agreement (Fig. 3). The data of (Michel et al., 1997) are surprisingly higher by a factor of five. The TENDL-2013 follows the trend of the experimental data but gives lower values.

#### 4.1.3. Cross sections of $^{95g}\text{Nb}$

The measured cross-sections of the  $^{95g}\text{Nb}$  ( $T_{1/2} = 34.991$  d) are cumulative, as they are deduced from spectra taken after a cooling time resulting in nearly complete IT decay of  $^{95}\text{Nb}$  ( $T_{1/2} = 86.64$  h). The agreement with the earlier experimental data is acceptable for both experiments (Fig. 4). The results of the nuclear model code TALYS from the TENDL-2013 library are in good agreement with the experiments.

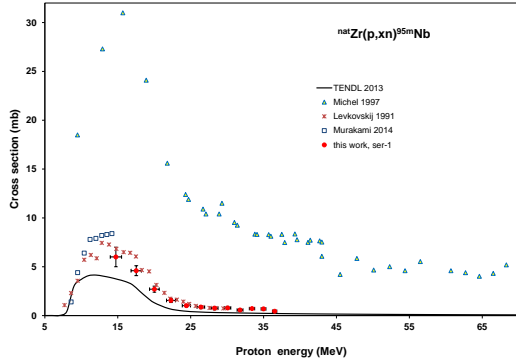


Figure 3: Excitation function of the  $^{nat}\text{Zr}(p,x)^{95m}\text{Nb}$  reaction

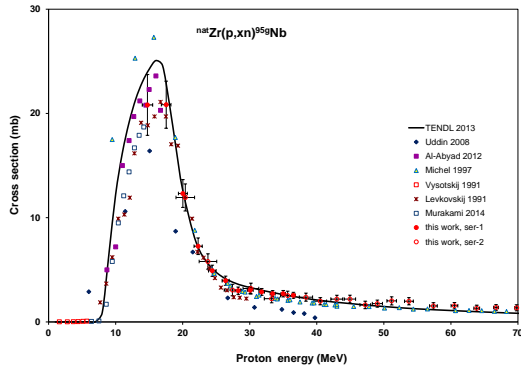


Figure 4: Excitation function of the  $^{nat}\text{Zr}(p,x)^{95g}\text{Nb}$  reaction

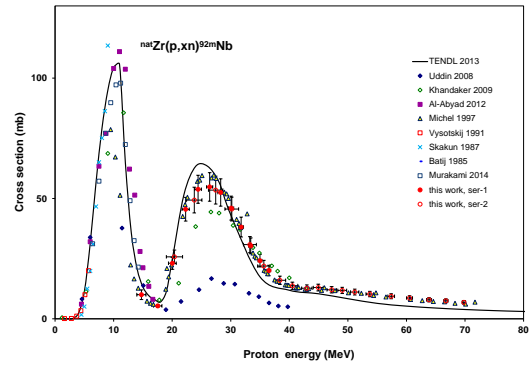


Figure 5: Excitation function of the  $^{nat}\text{Zr}(p,x)^{92m}\text{Nb}$  reaction

#### 4.1.4. Cross sections of $^{92m}\text{Nb}$

The half-life of the ground state of the  $^{92}\text{Nb}$  is very long ( $T_{1/2} = 3.47 \cdot 10^7$  a) and  $^{92g}\text{Nb}$  can hence be considered as stable in our experimental conditions. The isomeric state  $^{92m}\text{Nb}$  ( $T_{1/2} = 10.15$  d) has no IT, but decays directly to stable  $^{92}\text{Zr}$ . Our results for both experiments are in acceptable agreement with the earlier experimental results and with the data in TENDL-2013 (Fig. 5).

#### 4.1.5. Cross sections of $^{91m}\text{Nb}$

The very long-lived ground state of  $^{91}\text{Nb}$  ( $T_{1/2} = 6800$  a) has no measurable gamma lines. We obtained some results for the activation cross sections of the shorter-lived isomeric state ( $T_{1/2} = 60.86$  d), mostly from the high energy irradiation. Our data show large uncertainties due to the low statistics. The agreement with the earlier experimental results is acceptable (Fig. 6). The TENDL-2013 prediction overestimates the experimental data.

#### 4.1.6. Cross sections of $^{90}\text{Nb}$

The cross-sections for production of  $^{90g}\text{Nb}$  ( $T_{1/2} = 14.6$  h) obtained in the VUB experiment are shown in Fig. 7. The cross sections include, apart from the direct production, the contribution through IT decay (100%) of the 18.8 s half-life isomeric state. The agreement with the earlier experimental results is good, except for the data of (Kondratev et al., 1991; Blosser and Handley, 1955; Birjukov et al., 1979; Al-Abyad et al., 2012) (Fig. 7). The TENDL-2013 results are well representing the energy dependence of the contributions of the different reactions and their maximum values.

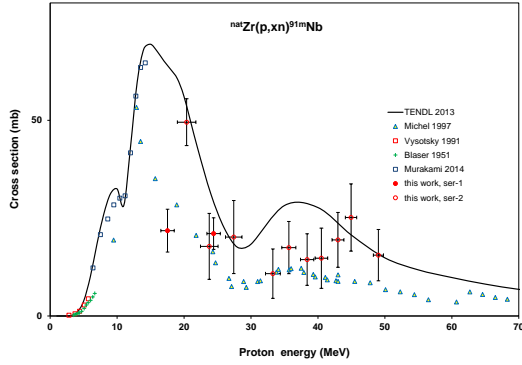


Figure 6: Excitation function of the  $^{nat}\text{Zr}(p,x)^{91m}\text{Nb}$  reaction

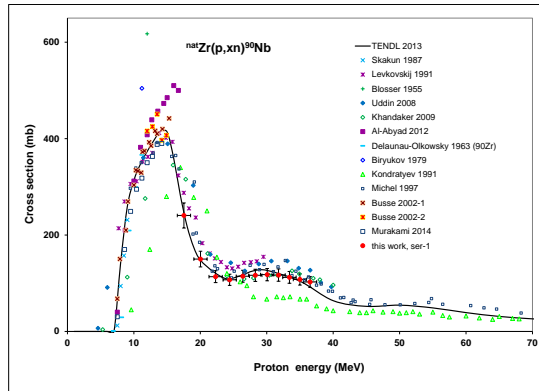


Figure 7: Excitation function of the  $^{nat}\text{Zr}(p,x)^{90}\text{Nb}$  reaction

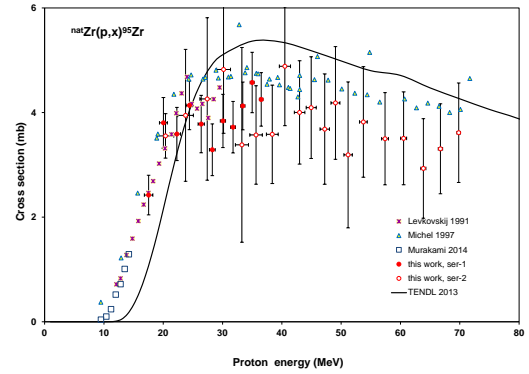


Figure 8: Excitation function of the  $^{nat}\text{Zr}(p,x)^{95}\text{Zr}$  reaction

#### 4.1.7. Cross sections of $^{95}\text{Zr}$

The radionuclide  $^{95}\text{Zr}$  ( $T_{1/2} = 64.032$  d) is formed directly through the  $^{96}\text{Zr}(p,pn)$  reaction and indirectly from the decay of the short-lived parent  $^{95}\text{Y}$  ( $T_{1/2} = 10.3$  min) produced via the  $^{96}\text{Zr}(p,2p)$  reaction. The agreement with earlier experimental data and with the TENDL-2013 predictions is acceptable for our 2 new experiments (Fig. 8).

#### 4.1.8. Cross sections of $^{89}\text{Zr}$

The cross sections for  $^{89}\text{Zr}$  ( $T_{1/2} = 78.41$  h) production include, apart from the direct (p,pxn) processes on different stable Zr isotopes, also the contributions from the decay of the short-lived metastable parent  $^{89m}\text{Zr}$  ( $T_{1/2} = 4.161$  min) and the decay of  $^{89}\text{Nb}$  ( $T_{1/2} = 66$  min). Our data from both experiments do not support the low cross section values of (Khandaker et al., 2009) and the TENDL-2013 predictions near in the 20-30 MeV energy range but are in agreement with the other literature values (Fig. 9).

#### 4.1.9. Cross sections of $^{88}\text{Zr}$

The measured cross-sections for  $^{88}\text{Zr}$  ( $T_{1/2} = 83.4$  d) production contain the direct formation and contributions from the decay of the two states of the short-lived parent  $^{88m,g}\text{Nb}$  ( $T_{1/2} = 7.78$  min and 14.55 min). Our both experimental data sets support the high maximum as found by (Michel et al., 1997). The agreement with the TENDL-2013 is acceptable (Fig. 10).

#### 4.1.10. Cross sections of $^{86}\text{Zr}$

The radionuclide  $^{86}\text{Zr}$  (16.5 h) was produced directly and from the decay of the two states of  $^{86m,g}\text{Nb}$  ( $T_{1/2}$

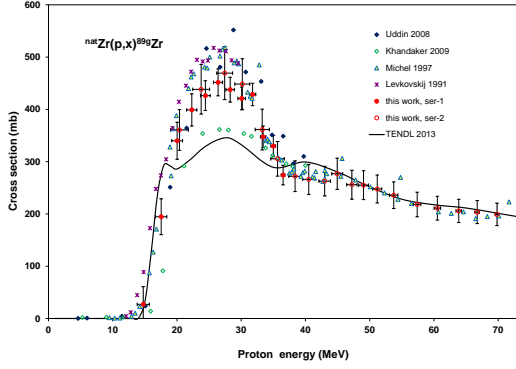


Figure 9: Excitation function of the  $^{nat}\text{Zr}(p,x)^{89}\text{Zr}$  reaction

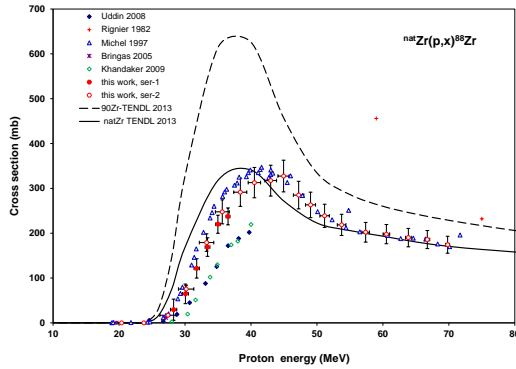


Figure 10: Excitation function of the  $^{nat}\text{Zr}(p,x)^{88}\text{Zr}$  reaction

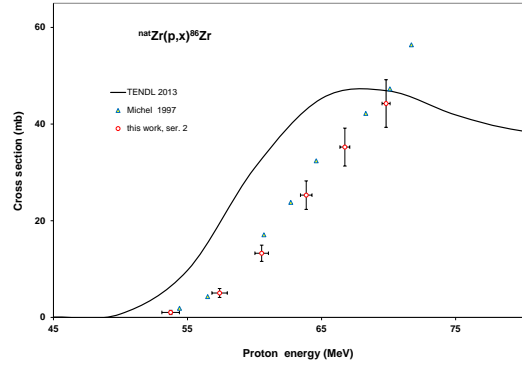


Figure 11: Excitation function of the  $^{nat}\text{Zr}(p,x)^{86}\text{Zr}$  reaction

= 56.3 s and 88 s). Our data agree with the experimental data of (Michel et al., 1997) and are lower than the TENDL-2013 results (Fig. 11).

#### 4.1.11. Cross sections of $^{88}\text{Y}$

The cross sections of  $^{88}\text{Y}$  ( $T_{1/2} = 106.627$  d) were obtained from the first spectra measured after EOB in order to minimize the contribution from the decay of the  $^{88}\text{Zr}$  parent nuclide with similar half-life ( $T_{1/2} = 83.4$  d). Up to 22-25 MeV no contribution from decay (also not from parent  $^{88}\text{Nb}$ ). Decay contribution does exist at higher energies. To get independent cross sections, the contribution from the decay of  $^{88}\text{Zr}$  was subtracted based on the measured counts at 393 keV, resulting in corrections on the count rate of the independent 898 keV  $\gamma$ -line. Unfortunately, because of the relative long half-life and the shorter measuring time the  $^{88}\text{Y}$  peak could not be evaluated reliably from the high energy spectra. The agreement is acceptable (Fig. 12).

#### 4.1.12. Cross sections of $^{87m}\text{Y}$

The radionuclide  $^{87}\text{Y}$  has a metastable state  $^{87m}\text{Y}$  ( $T_{1/2} = 13.37$  h) that decays completely to the ground state  $^{87g}\text{Y}$  ( $T_{1/2} = 79.8$  h). The cross-sections for  $^{87m}\text{Y}$  (Fig.13) contain the contributions from both the direct production through (p,2pxn) reactions and the decay of  $^{87g}\text{Zr}$  ( $T_{1/2} = 1.68$  h,  $\varepsilon = 100$  %) that could not be assessed independently. As the reaction with lowest threshold to produce  $^{87}\text{Zr}$  is the  $^{90}\text{Zr}(p,p3n)$  process with a threshold above 33 MeV, the cross sections at low energy are due to emission of clusters ( $\alpha$ -particles) in the direct reaction. The results of our two new data sets

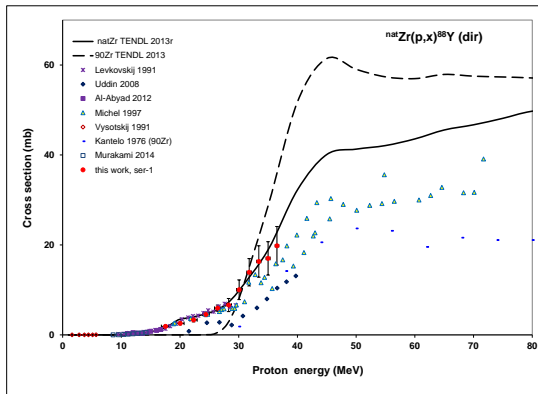


Figure 12: Excitation function of the  $^{nat}\text{Zr}(p,x)^{88}\text{Y}$  reaction

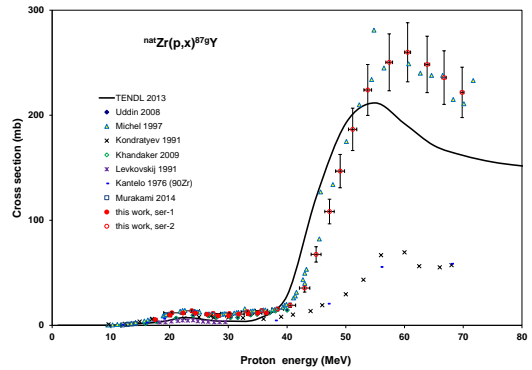


Figure 14: Excitation function of the  $^{nat}\text{Zr}(p,x)^{87g}\text{Y}$  reaction

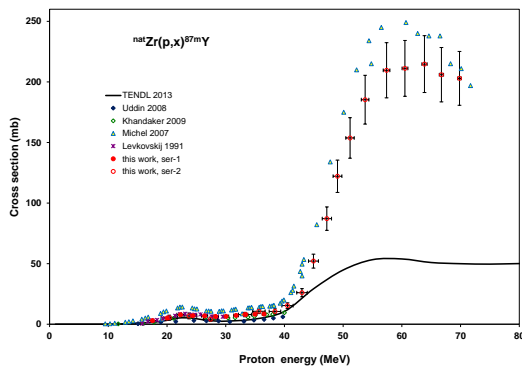


Figure 13: Excitation function of the  $^{nat}\text{Zr}(p,x)^{87m}\text{Y}$  reaction

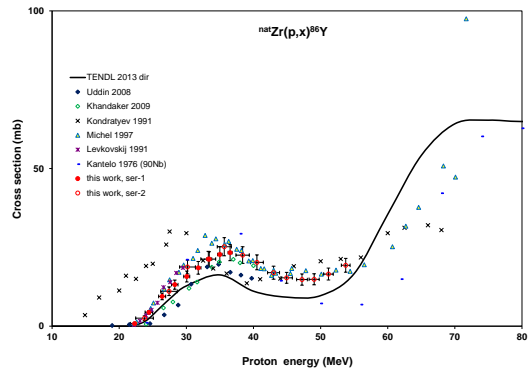


Figure 15: Excitation function of the  $^{nat}\text{Zr}(p,x)^{86}\text{Y}$  reaction

agree well with the earlier studies both in the low (cluster emission) and high energy (individual nucleons) regions. The TENDL-2013 predictions underestimate by a factor of 6 the high energy individual nucleons emission.

#### 4.1.13. Cross sections of $^{87g}\text{Y}$

The cumulative cross sections of  $^{87g}\text{Y}$  ( $T_{1/2} = 79.8$  h) contain the direct production, the contribution from the decay of  $^{87m}\text{Y}$  isomeric state ( $T_{1/2} = 13.37$  h) and contributions from the decay of parents  $^{87g}\text{Zr}$  ( $T_{1/2} = 1.6$  h) and  $^{87m}\text{Zr}$  ( $T_{1/2} = 14$  s, IT: 100 %). The same remark concerning the contributions of clusters and individual nucleons emissions as for  $^{87m}\text{Y}$  are valid. The agreement with the earlier experimental data and with

TENDL-2013 is shown in Fig. 14.

#### 4.1.14. Cross sections of $^{86}\text{Y}$

The production cross sections for  $^{86g}\text{Y}$  ( $T_{1/2} = 14.74$  h) contain the direct production and the contribution from the decay of short-lived isomeric state  $^{86m}\text{Y}$  ( $T_{1/2} = 48$  min, IT 99.3 %). The contributions from the decay of  $^{86}\text{Zr}$  at high energies (see Fig. 11) were subtracted. The experimental and theoretical data are shown in Fig. 15.

## 5. Integral yields

Thick target yields (integrated yield for a given incident energy down to the reaction threshold) were calcu-

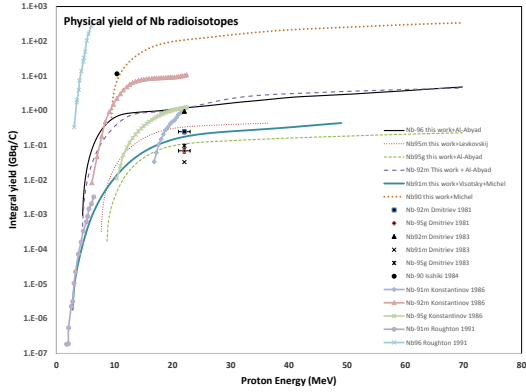


Figure 16: Integral yields for production of  $^{96}\text{Nb}$ ,  $^{95}\text{Nb}$ ,  $^{95g}\text{Nb}$ ,  $^{92m}\text{Nb}$ ,  $^{91m}\text{Nb}$ ,  $^{90}\text{Nb}$  deduced from the excitation functions

lated from fitted curves to our experimental cross section data. The results for physical yields (production rates) (Bonardi, 1987) are presented in Figs. 16-18. Some earlier experimental thick target yield data found in the literature are also presented.

## 6. Production of medically relevant radioisotopes by charged particle induced reactions on Zr targets

Among the studied activation products the radionuclides  $^{90}\text{Nb}$ ,  $^{95}\text{Nb}$ ,  $^{89}\text{Zr}$ ,  $^{88}\text{Y}$  are of interest in nuclear medicine. The possible production routes for these nuclides using medium energy cyclotrons are shown in Table 6 and will be discussed for each nuclide separately with the aim to identify the possible role of proton induced reactions on Zr studied in this work. Nuclear reactions having low production yields, or resulting carrier added, low specific activity product are not included in the comparison.

### 6.1. Production routes of $^{90}\text{Nb}$

The  $^{90}\text{Nb}$  ( $T_{1/2}=23.35$  h) can be produced at low energy accelerators in various ways on Zr or Y targets ( $^{90}\text{Zr}(p,n)^{90}\text{Nb}$ ,  $^{90}\text{Zr}(d,2n)^{90}\text{Nb}$ ,  $^{91}\text{Zr}(p,2n)^{90}\text{Nb}$ ,  $^{89}\text{Y}(\alpha,2n)^{90}\text{Nb}$ ,  $^{89}\text{Y}(^3\text{He},n)^{90}\text{Nb}$ , see Table 6). Out of them only the  $^{90}\text{Zr}(p,n)$  and  $^{89}\text{Y}(^3\text{He},n)$  reactions on enriched targets give products with high radionuclidic purity, as by limitations of the incident energy, reactions leading to Nb radionuclides with lower mass number can be suppressed (Q-value of  $^{90}\text{Zr}(p,2n)$  reaction is -17.002 MeV). In the case of natural Zr targets long-lived, higher mass Nb radionuclides are produced

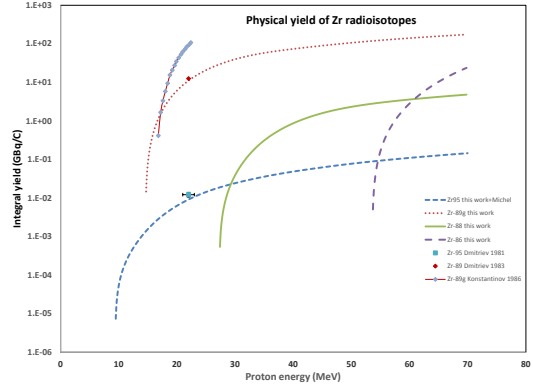


Figure 17: Integral yields for production of  $^{95}\text{Zr}$ ,  $^{89}\text{Zr}$ ,  $^{88}\text{Zr}$ ,  $^{86}\text{Zr}$  deduced from the excitation functions

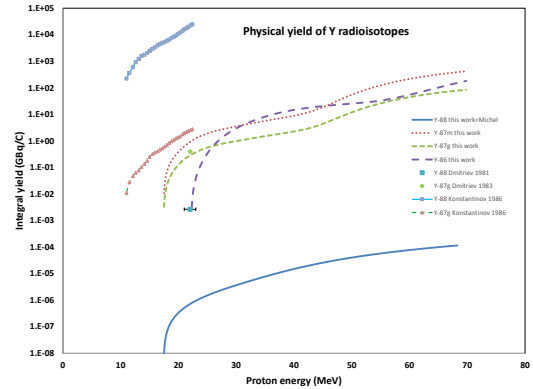


Figure 18: Integral yields for production of  $^{88}\text{Y}$ ,  $^{87m}\text{Y}$ ,  $^{87g}\text{Y}$ ,  $^{86}\text{Y}$  deduced from the excitation functions



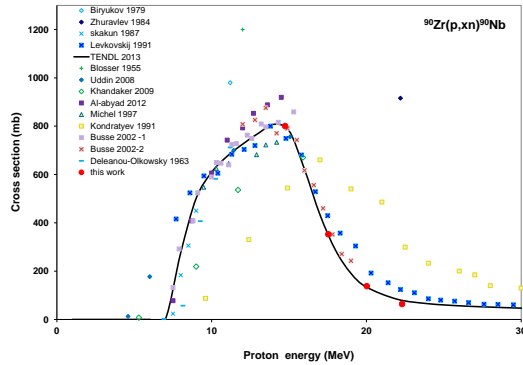


Figure 19: Excitation function of the  $^{90}\text{Zr}(p,x)^{90}\text{Nb}$  reaction

simultaneously e.g.  $^{91m}\text{Nb}$  ( $T_{1/2}=60.86$  d) and  $^{91g}\text{Nb}$  ( $T_{1/2} = 680$  a) through the  $^{91}\text{Zr}(p,n)$  reaction. In Fig. 19 we reproduce the experimental cross section data of the  $^{90}\text{Zr}(p,n)$  reaction (obtained on enriched  $^{90}\text{Zr}$  or derived from measurements on  $^{nat}\text{Zr}$  (corrected by the TENDL  $^{91}\text{Zr}(p,2n)^{90}\text{Nb}$  data), threshold of  $^{91}\text{Zr}(p,2n)^{90}\text{Nb}$  reaction is -14.244 MeV). As it is shown the TENDL-2013 data reproduce well the experimental values for this reaction cross section. In Fig. 20 for discussion we reproduce the excitation functions for  $^{90}\text{Zr}(d,2n)^{90}\text{Nb}$  and  $^{89}\text{Y}(\alpha,2n)^{90}\text{Nb}$  based on experimental data and for  $^{90}\text{Zr}(p,n)^{90}\text{Nb}$  and  $^{89}\text{Y}(\alpha,3n)^{90}\text{Nb}$  reactions taken from the TENDL-2013 library. The deduced integral yields are shown in Fig. 21. It is clear from the cross sections and the integral yields, that the  $^{90}\text{Zr}(p,n)^{90}\text{Nb}$  reaction is the method of choice but requires highly enriched targets.

## 6.2. Production routes of $^{95}\text{Nb}$

The radionuclide  $^{95}\text{Nb}$  ( $T_{1/2}=3.61$  d) can be produced with high specific activity and free from contaminants (if suitable cooling time is applied) with  $^{96}\text{Zr}(p,2n)$ ,  $^{94}\text{Zr}(d,n)$  and  $^{96}\text{Zr}(d,3n)$  reactions. The cross sections from experiments on enriched targets or the values derived from irradiations on  $^{nat}\text{Zr}$  targets are shown on Fig. 22 together with the data from the TENDL-2013 library. All of these reactions require highly enriched targets to obtain an end product with high specific activity and minimal contaminations. The  $^{96}\text{Zr}(p,2n)$  reaction is the most promising, considering both the yield and the required accelerator energy.

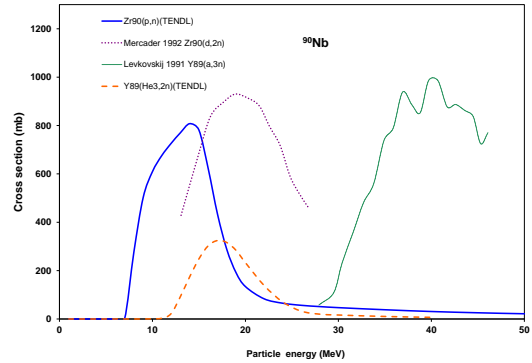


Figure 20: Excitation function of the  $^{90}\text{Zr}(p,n)^{90}\text{Nb}$ ,  $^{90}\text{Zr}(d,2n)^{90}\text{Nb}$ ,  $^{89}\text{Y}(\alpha,3n)^{90}\text{Nb}$  and  $^{89}\text{Y}(\alpha,2n)^{90}\text{Nb}$  reactions

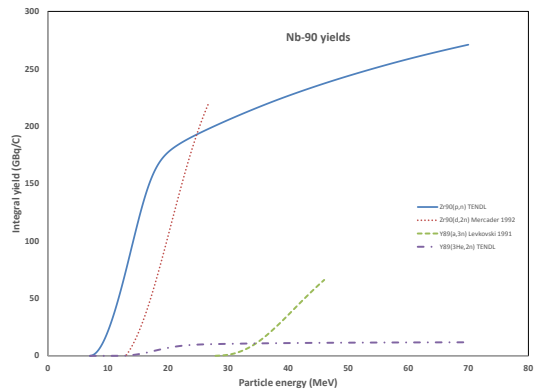


Figure 21: Integral yields of the  $^{90}\text{Zr}(p,n)^{90}\text{Nb}$ ,  $^{90}\text{Zr}(d,2n)^{90}\text{Nb}$ ,  $^{89}\text{Y}(\alpha,3n)^{90}\text{Nb}$  and  $^{89}\text{Y}(\alpha,2n)^{90}\text{Nb}$  reactions

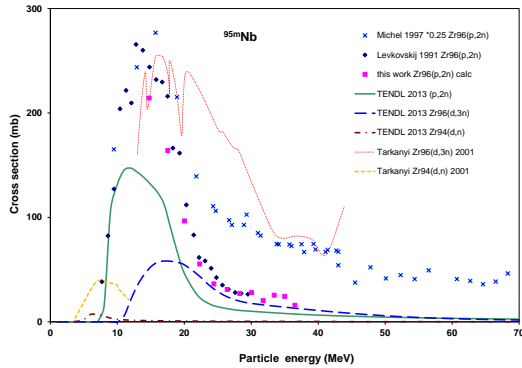


Figure 22: Excitation function of the  $^{96}\text{Zr}(p,2n)$ ,  $^{94}\text{Zr}(d,n)$  and  $^{96}\text{Zr}(d,3n)$  reactions

### 6.3. Production routes of $^{89}\text{Zr}$

The low and medium energy production routes for  $^{89}\text{Zr}$  ( $T_{1/2}=78.41$  h) are  $^{89}\text{Y}(p,n)^{89}\text{Zr}$  and  $^{89}\text{Y}(d,2n)^{89}\text{Zr}$  as direct routes and  $^{90}\text{Zr}(p,2n)^{89}\text{Nb}-^{89}\text{Zr}$  as indirect route. A large number of experimental data sets exist for the direct (p,n) and (d,2n) reactions (see Fig. 23 and 24, the experimental data were taken from EXFOR). Both reactions result in non-carrier added (nca) product and the yttrium has only one stable isotope. The (p,n) route hence seems to be the most beneficial, both in yield and the required accelerator characteristics. In principle  $^{89}\text{Zr}$  can be produced carrier free indirectly by using Zr targets through the  $^{90}\text{Zr}(p,2n)^{89}\text{Nb}-^{89}\text{Zr}$  reaction. No experimental data are available for this reaction. The theoretical data from TENDL-2013 are shown in Fig. 23. When considering integral yields the  $^{90}\text{Zr}(p,2n)^{89}\text{Nb}-^{89}\text{Zr}$  indirect production route is the most productive, but it requires highly enriched targets and only short irradiations are possible due to the short half-life of the isomeric states of the  $^{89}\text{Nb}$  ( $^{89m}\text{Nb}$   $T_{1/2} = 66$  min,  $^{89g}\text{Nb}$   $T_{1/2} = 2.13$  h) and the need to separate the Nb from the Zr target to obtain high specific activity NCA end-product.

### 6.4. Production routes of $^{88}\text{Y}$

The direct production of  $^{88}\text{Y}$  ( $T_{1/2} = 106.627$  d) is possible through the  $^{nat}\text{Sr}(p,xn)$ ,  $^{nat}\text{Sr}(d,xn)$ ,  $^{nat}\text{Rb}(\alpha,xn)$ ,  $^{nat}\text{Zr}(p,x)$  and  $^{90}\text{Zr}(p,x)$  reactions. The excitation functions for the direct production are shown in Figs. 25-26 (the data were taken from EXFOR or from TENDL-2013 for the (d,xn) reaction) and in Fig. 12. By using  $^{nat}\text{Zr}(p,x)$  the cross section is low and

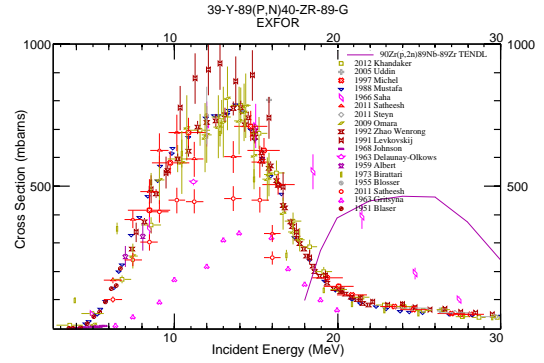


Figure 23: Excitation function of the  $^{89}\text{Y}(p,n)^{89}\text{Zr}$  reaction, plotted together with the  $^{90}\text{Zr}(p,2n)^{89}\text{Nb}$  reaction cross section also producing the  $^{89}\text{Zr}$  isotope

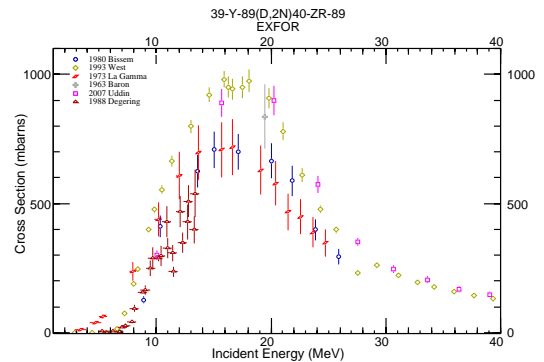


Figure 24: Excitation function of the  $^{89}\text{Y}(d,2n)^{89}\text{Zr}$  reaction

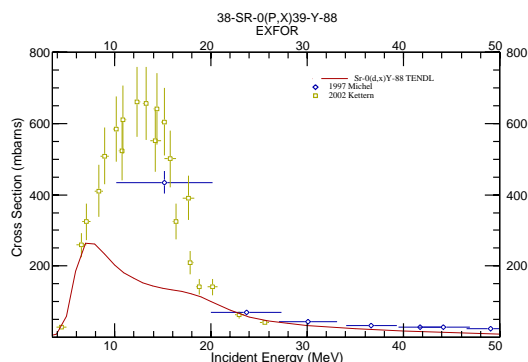


Figure 25: Excitation function of the  $\text{natSr}(p,x)^{88}\text{Y}$  and  $\text{natSr}(d,x)^{88}\text{Y}$  reaction

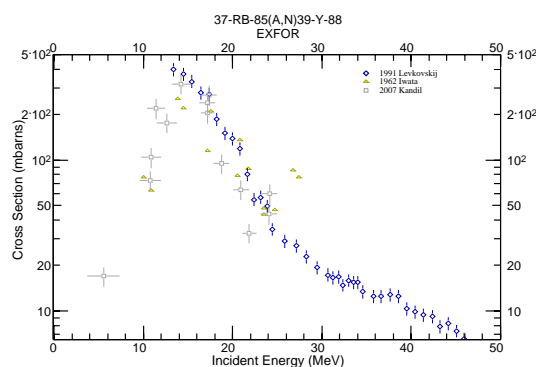


Figure 26: Excitation function of  $^{85}\text{Rb}(n)$  reaction

long-lived  $^{91}\text{Y}$  (58.51 d) is produced simultaneously. To get high radionuclidic purity highly enriched  $^{90}\text{Zr}$  should be used. As Rb has only two stable isotopes ( $^{85}\text{Rb}$ :72.165 % and  $^{87}\text{Rb}$ :27.83%) and  $^{90}\text{Y}$  with a significantly shorter half-life is produced by  $(\alpha,n)$  reaction, natural Rb targets can be used. However the limitation on incoming  $\gamma$ -energy is important for avoiding production of stable  $^{89}\text{Y}$  through  $^{87}\text{Rb}(\alpha,2n)$ , which would decrease specific activity. The maximum production cross section on natRb will hence be only around 230 mb. The indirect production routes include the  $\text{natZr}(p,x)^{88}\text{Zr}$ - $^{88}\text{Y}$ ,  $^{90}\text{Zr}(p,x)^{88}\text{Zr}$ - $^{88}\text{Y}$ ,  $^{89}\text{Y}(p,2n)$   $^{88}\text{Zr}$ - $^{88}\text{Y}$  reactions. The excitation functions are shown in Fig. 10 and Fig. 27 (the experimental data for  $^{89}\text{Y}$  were taken from EXFOR). By using Zr target the production requires highly enriched  $^{90}\text{Zr}$  material. In case of natural composition other long-lived Zr radioisotopes as  $^{93}\text{Zr}$  ( $T_{1/2} = 1.61106$  a) and  $^{95}\text{Zr}$  ( $T_{1/2} = 64.032$  d) are produced simultaneously, followed by Y decay product. In case  $^{90}\text{Zr}$  target the  $^{88}\text{Y}$  is produced directly, simultaneously with  $^{88}\text{Zr}$  via  $(p,2pxn)$  reaction, which can be separated after EOB (the other Y radio-products are short-lived). Comparison of the two production routes shows, that the  $(p,2n)$  reaction on monoisotopic yttrium has advantages as no enriched targets are required, and the required beam energy is lower up to 30 MeV (in the range of commercial medium energy cyclotrons).

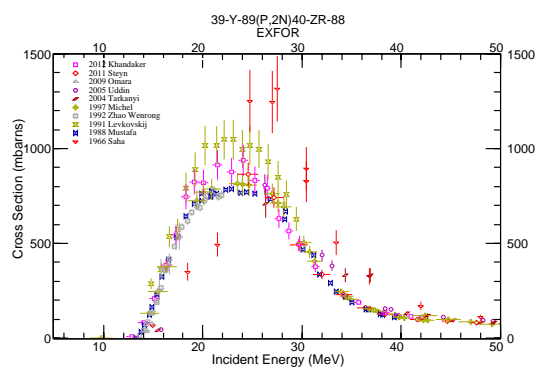


Figure 27: 27. Excitation function of the  $^{89}\text{Y}(p,2n)^{88}\text{Zr}$  reaction

## 7. Summary

We present experimental activation cross sections for production of  $^{96}\text{Nb}$ ,  $^{95}\text{Nb}$ ,  $^{95g}\text{Nb}$ ,  $^{92m}\text{Nb}$ ,  $^{91m}\text{Nb}$ ,  $^{90}\text{Nb}$ ,

$^{95}\text{Zr}$ ,  $^{89}\text{Zr}$ ,  $^{88}\text{Zr}$ ,  $^{86}\text{Zr}$ ,  $^{88}\text{Y}$ ,  $^{87m}\text{Y}$ ,  $^{87g}\text{Y}$ ,  $^{86}\text{Y}$  on zirconium measured up to 70 MeV proton energy. The agreement between the new and the earlier experimental data (except for a few cases) is acceptable. TALYS 1.4 based model results in TENDL-2013 library describe well the experimental results. For production of the medically relevant radionuclides  $^{90}\text{Nb}$ ,  $^{95}\text{Nb}$ ,  $^{89}\text{Zr}$ ,  $^{88}\text{Y}$  different alternative routes were compared and discussed. For production of  $^{90}\text{Nb}$  and  $^{95}\text{Nb}$  the proton induced reactions on enriched  $^{90}\text{Zr}$  and  $^{96}\text{Zr}$ , respectively, are preferred compared to other routes. For production of  $^{89}\text{Zr}$  and  $^{88}\text{Y}$  the proton and deuteron induced reactions on  $^{nat}\text{Y}$  from all points of view are more practical.

## 8. Acknowledgements

This work was partly performed in the frame of the HAS-FWO Vlaanderen (Hungary-Belgium) project as well as in cooperation with the Tohoku University, Sendai, Japan. The authors acknowledge the support of the research project and the respective institutions in providing the beam time and experimental facilities.

## References

- Abe, K., Iizuka, A., Hasegawa, A., Morozumi, S., 1984. Induced radioactivity of component materials by 16-mev protons and 30-mev alpha-particles. *Journal of Nuclear Materials* 123 (1-3), 972–976.
- Al-Abyad, M., Abdel-Hamid, A. S., Tárkányi, F., Ditrói, F., Takács, S., Seddik, U., Bashter, I. I., 2012. Cross-section measurements and nuclear model calculation for proton induced nuclear reaction on zirconium. *Applied Radiation and Isotopes* 70 (1), 257–262.
- Batij, V. G., A., S. A., Rakivnenko, Y. N., Rastrepin, P. A., 1985. Investigation of  $^{90}\text{Zr}(p,n)^{90m,g}\text{Nb}$ ,  $^{92}\text{Zr}(p,n)^{92m}\text{Nb}$  and  $^{96}\text{Zr}(p,n)^{96}\text{Nb}$  reactions in 44-9 mev energy range. In: 35th Annual Conference on Nuclear Spectroscopy and Structure of Atomic Nuclei. p. 85.
- Birjukov, N. S., Zhuravrev, B. V., Rudenko, A. P., Salnikov, O. A., Trykova, V. I., 1979. Neutrons from (p,n) reactions on  $^{90,91,94}\text{Zr}$ . *Yadernaya Fizika* 29 (6), 1443.
- Blaser, J., Boehm, F., Marimier, P., Scherrer, P., 1951. Anregungsfunktionen und wirkungsquerschnitte der (p,n)-reaktion (ii). *Helvetica Physica Acta* 24, 441–445.
- Blosser, H., Handley, T., 1955. Survey of (p,n) reactions at 12 mev. *Phys. Rev.* 100, 1340–1344.
- Bonardi, M., 1987. The contribution to nuclear data for biomedical radioisotope production from the milan cyclotron facility.
- Bringas, F., Yamashita, M. T., Goldman, I. D., Pascholati, P. R., Sciani, V., 2005. Measurement of proton-induced reaction cross sections in ti, ni and zr near the threshold. In: Haight, R. C., Chadwick, M. B., Kawano, T., Talou, P. (Eds.), *Intern.Conf.Nuclear Data for Science and Technology*. Vol. 769. AIP, pp. 1374–1377.
- Broeders, C. H. M., Konobeyev, A. Y., 2007. Systematics of (p,alpha) (p,n alpha), and (p,np) reaction cross-sections. *Applied Radiation and Isotopes* 65 (11), 1249–1264.
- Busse, S., Rosch, F., Qaim, S. M., 2002. Cross section data for the production of the positron emitting niobium isotope nb-90 via the zr-90(p, n)-reaction. *Radiochimica Acta* 90 (1), 1–5.
- Cai, C. H., 2006. Mend - a program for calculating the complete set of nuclear data of medium-heavy nuclei in a medium-low energy region. *Nuclear Science and Engineering* 153 (1), 93–97.
- Delaunau-Olkowsky, J., Strohal, P., Cindro, N., 1963. Total reaction cross section of proton induced reactions. *Nuclear Physics* 47, 266.
- Dityuk, A. I., Konobeyev, A. Y., Lunev, V. P., Shubin, Y. N., 1998. New version of the advanced computer code alice-ippe. Tech. rep., IAEA.
- Dmitriev, P. P., 1983. Systematics of nuclear reaction yields for thick target at 22 mev proton energy. *Vop. At. Nauki i Tekhn., Ser.Yadernye Konstanty* 57, 2.
- Dmitriev, P. P., Molin, G. A., 1981. Radioactive nuclide yields for thick target at 22 mev proton energy. *Vop. At. Nauki i Tekhn., Ser.Yadernye Konstanty* 44 (5), 43.
- Gorpinich, O. K., Kondratev, S. N., Kuzmenko, V. A., Lobach, Y. N., 1988. Excitation functions of (p, 4pxn) reaction on zr nuclei at proton energy up to 70 mev. In: 38th Ann. Conf. Nucl. Spectrosc. Struct. At. Nuclei. p. 310.
- Gul, K., Hermanne, A., Mustafa, M. G., Nortier, F. M., Oblozinsky, P., Qaim, S. M., Scholten, B., Shubin, Y. N., Takács, S., Tárkányi, F., Zhuang, Y., 2001. Charged particle cross-section database for medical radioisotope production diagnostic radioisotopes and monitor reactions. charged particle cross-section database for medical radioisotope production: diagnostic radioisotopes and monitor reactions. vienna, iaea. iaea-tecdoc-1211, <http://www.nds.or.at/medical>.
- IAEA, 2001. Nuclear data for the production of therapeutic radionuclides. Tech. rep., IAEA.
- IAEA, 2004. Fusion evaluated nuclear data library fendl 3.0.
- IAEA, 2008. Exfor formats description for users (exfor basics) iaea-nds-206.
- IAEA, 2012-2016. Crp on nuclear data for charged-particle monitor reactions and medical isotope production.
- IAEA-NDS, 2010. Thin layer activation (tla) technique for wear measurement.
- Isshiki, M., Fukuda, Y., Igaki, K., 1984. Proton activation-analysis of trace impurities in purified cobalt. *Journal of Radioanalytical and Nuclear Chemistry* 82 (1), 135–142.
- Kantelo, M. V., Hogan, J. J., 1976. Charged-particle emission in reactions of zr-90 with 10-86-mev protons. *Physical Review C* 14 (1), 64–74.
- Khandaker, M. U., Kim, K., Lee, M. W., Kim, K. S., Kim, G. N., Cho, Y. S., Lee, Y. O., 2009. Experimental determination of proton-induced cross-sections on natural zirconium. *Applied Radiation and Isotopes* 67 (7-8), 1341–1347.
- Kondratev, S. N., Kuzmenko, V. A., Lobach, Y. N., Prokopenko, V. F., Sklyarenko, V. D., Tokarevskii, V. V., 1991. Production cross-section of radionuclides at interaction zr nuclei with 70 mev protons. *Atomnaya Energiya* 71, 325.
- Koning, A. J., Hilaire, S., Duijvestijn, M. C., 2007. Talys-1.0.
- Koning, A. J., Rochman, D., van der Marck, S., Kopecky, J., Sublet, J. C., Pomp, S., Sjostrand, H., Forrest, R., Bauge, E., Henriksson, H., Cabellos, O., Goriely, S., Leppanen, J., Leeb, H., Plompen, A., Mills, R., 2012. Tendl-2013: Talys-based evaluated nuclear data library.
- Konstantinov, I. O., Dmitriev, P. P., Bolotskikh, V. I., 1986. Activation of zirconium, niobium, and tantalum in a cyclotron. *Soviet Atomic Energy* 60 (5), 390–395.
- Kuzmenko, V. A., Lobach, Y. N., Prokopenko, V. S., Sklyarenko, V. D., Tokarevskiy, V. V., 1987. Excitation functions of long-lived radionuclides under irradiation of zirconium by protons, deuterons and alpha-particles. In: 37th Ann.Conf.Nucl.Spectrosc.Struct.At.Nuclei. p. 311.
- Levkovskii, V. N., 1991. The cross-sections of activation of nuclides of middle-range mass (A=40-100) by protons and alpha particles

- of middle range energies ( $E=10\text{-}50\text{ MeV}$ ). Inter-Vesny, Moscow.
- Michel, R., Bodemann, R., Busemann, H., Daunke, R., Gloris, M., Lange, H. J., Klug, B., Krins, A., Leya, I., Lupke, M., Neumann, S., Reinhardt, H., SchnatzButtgen, M., Herpers, U., Schiekel, T., Sudbrock, F., Holmqvist, B., Conde, H., Malmborg, P., Suter, M., DittrichHannen, B., Kubik, P. W., Synal, H. A., Filges, D., 1997. Cross sections for the production of residual nuclides by low- and medium-energy protons from the target elements c, n, o, mg, al, si, ca, ti, v, mn, fe, co, ni, cu, sr, y, zr, nb, ba and au. Nuclear Instruments & Methods in Physics Research Section B-Beam Interactions with Materials and Atoms 129 (2), 153–193.
- Muminov, V. A., Mukhammedov, S., Vasidov, A., 1980. Possibilities of proton-activation analysis for determining the content of elements from short-lived radionuclides. Soviet Atomic Energy 49 (2), 540–544.
- Murakami, M., Haba, H., Goto, S., Kanaya, J., Kudo, H., 2014. Production cross sections of niobium and tantalum isotopes in proton-induced reactions on natzr and natfh up to 140;mev. Applied Radiation and Isotopes 90 (0), 149–157.
- Naik, H., Goswami, A., Kim, G., Kim, K., Yang, S. C., Sahid, M., Zaman, M., Lee, M., Shin, S. G., Cho, M. H., 2014. Independent isomeric-yield ratio of nb-89m,nb-g from nb-93( $\gamma$ , 4n), zr-nat(p, xn), and y-89( $\alpha$ , 4n) reactions. Journal of Radioanalytical and Nuclear Chemistry 299 (3), 1335–1343.
- Nickles, R. J., 1991. A shotgun approach to the chart of the nuclides. Acta Radiol. Suppl. 376, 69–71.
- NuDat, 2014. Nudat2 database (2.6).
- of-Weights-and Measures, I.-B., 1993. Guide to the expression of uncertainty in measurement, 1st Edition. International Organization for Standardization, GenÈve, Switzerland.
- Regnier, S., Lavielle, B., Simonoff, M., Simonoff, G. N., 1982. Nuclear-reactions in rb, sr, y, and zr targets. Physical Review C 26 (3), 931–943.
- Ren, W. T., Zhang, Z. J., Han, Y. L., 2011. Calculation and analysis of cross-sections for p+ zr reactions up to 200 mev. Nuclear Instruments & Methods in Physics Research Section B-Beam Interactions with Materials and Atoms 269 (4), 472–483.
- Roughton, N. A., Fritts, M. R., Peterson, R. J., Zaidins, C. S., Hansen, C. J., 1979. Thick-target measurements and astrophysical thermonuclear reaction rates: Proton-induced reactions. Atomic Data and Nuclear Data Tables 23, 177–194.
- Sadeghi, M., Kakavand, T., Taghilo, M., 2011. Calculation of excitation function to produce zr-89 via various nuclear reactions by alice/ash code. International Journal of Modern Physics E-Nuclear Physics 20 (8), 1775–1786.
- Shubin, Y. N., Lunev, V. P., Konobeyev, A. Y., Dityuk, A. I., 1998. Mendl-2p protonreaction data library for nuclear activation (medium energy nuclear data library). Tech. rep., IAEA.
- Skakun, E. A., Batij, V. G., Rakivnenko, Y. N., Rastrepin, O. A., 1987. Excitation functions and isomer ratios for up-to-9 mev proton interactions with zr and mo isotope nuclei. Journal Soviet Nuclear Physics 46, 17.
- Tárkányi, F., Ditrói, F., Takács, S., Csikai, J., Mahunka, I., Uddin, M. S., Hagiwara, M., Baba, M., Ido, T., Hermanne, A., Sonck, M., Shubin, Y., Dityuk, A. I., 1985. Excitation functions for production of 88zr and 88y by proton and deuteron irradiation of mo, nb, zr, and y. In: Haight, R., Chadwick, M., Kawano, T., Talou, P. (Eds.), Intern.Conf.Nuclear Data for Science and Technology. Vol. 769. AIP Conf. Proc., p. 1658.
- Tárkányi, F., Hermanne, A., Takács, S., Ditrói, F., Dityuk, A. I., Shubin, Y. N., 2004. Excitation functions for production of radioisotopes of niobium, zirconium and yttrium by irradiation of zirconium with deuterons. Nuclear Instruments & Methods in Physics Research Section B-Beam Interactions with Materials and Atoms 217 (3), 373–388.
- Tárkányi, F., Takács, S., Gul, K., Hermanne, A., Mustafa, M. G., Nortier, M., Oblozinsky, P., Qaim, S. M., Scholten, B., Shubin, Y. N., Youxiang, Z., 2001. Charged particles cross-sections database for medical radioisotope production, beam monitors reactions.
- Tel, E., Aydin, A., Aydin, E. G., Kaplan, A., Yavas, O., Reyhancan, I. A., 2010. Newly developed semi-empirical formulas for (p, alpha) at 17.9 mev and (p, np) at 22.3 mev reaction cross-sections. Pramana-Journal of Physics 74 (6), 931–943.
- Uddin, M. S., Baba, M., Hagiwara, M., Tárkányi, E., Ditrói, F., 2007. Experimental determination of deuteron-induced activation cross sections of yttrium. Radiochimica Acta 95 (4), 187–192.
- Uddin, M. S., Hagiwara, M., Baba, M., Tárkányi, F., Ditrói, F., 2005. Experimental studies on excitation functions of the proton-induced activation reactions on yttrium. Applied Radiation and Isotopes 63 (3), 367–374.
- Uddin, M. S., Khandaker, M. U., Kim, K. S., Lee, Y. S., Lee, M. W., Kim, G. N., 2008. Excitation functions of the proton induced nuclear reactions on natural zirconium. Nuclear Instruments & Methods in Physics Research Section B-Beam Interactions with Materials and Atoms 266 (1), 13–20.
- Vysotsky, O. N., Gonchar, A. V., Gorpinich, O. K., Kondratev, S. N., Prokopenko, V. S., Rakitin, S. B., Sklyarenko, V. D., Tokarevsky, V. V., 1991. Excitation functions of reactions  $zr+p,d \rightarrow {}^{91m}nb, {}^{92m}nb, {}^{95}nb, {}^{96}nb, {}^{88}y$ . In: 41st Annual Conference on Nuclear Spectroscopy and Structure of Atomic Nuclei. p. 486.
- Ziegler, J. F., 2013. Srim-2013 <http://www.srim.org/#srim>.

Table 1: Summary of earlier experimental investigations on activation cross sections and yields of the proton induced nuclear reaction on zirconium. The investigated quantities of the nuclear reactions are indicated according to the conventions of the EXFOR system (IAEA, 2008).

Author	Target	Irradiation	Beam current measurement and monitor reaction	Separation method and measurement of activity	Nuclear reaction and measured quantity and number of measured data points	Covered energy range(MeV)
(Blaser et al., 1951)	$nat$ Zr nitrate	cyclotron stacked foil	$^{63}\text{Cu}(p,n)^{63}\text{Zn}$ $^{62}\text{Ni}(p,n)^{62}\text{Cu}$	Geiger-Müller counter	40-ZR-96(PN)41-NB-96,SIG, 15 40-ZR-92(PN)41-NB-92,SIG, 10 40-ZR-91(PN)41-NB-91-M,SIG, 12	2.73-6.67 3.5-6.67 3.5-6.66
(Blosser and Handley, 1955)	single foil	cyclotron	$^{63}\text{Cu}(p,n)^{63}\text{Zn}$	Geiger-Müller counter	40-ZR-90(PN)41-NB-90-G,M+,SIG,EXP,1	12.7
(Delaunau-Olkowsky et al., 1963)	$^{90}\text{Zr},^{91}\text{Zr},^{92}\text{Zr}$	cyclotron	$^{65}\text{Cu}(p,n)^{65}\text{Zn}$	$\gamma$ -NaI(Tl)	40-ZR-90(Pa)39-Y-87,SIG,EXP, 1 40-ZR-91(Pa)39-Y-88,SIG,EXP, 1 40-ZR-94(Pa)39-Y-91,SIG,EXP, 1	11.2 11.2 11.2
(Kantelo and Hogan, 1976)	$^{90}\text{Zr}$ -oxide	cyclotron single target	$^{63}\text{Cu}(p,n)^{63}\text{Zn}$ $^{65}\text{Cu}(p,x)^{64}\text{Cu}$	$\gamma$ -Ge (Li)	40-ZR-90(PX)39-Y-86-G,M+,SIG,EXP,1 40-ZR-90(PX)39-Y-87-G,M+,SIG,EXP,1 40-ZR-90(PX)39-Y-88, SIG,EXP,1 40-ZR-90(PX)39-Y-85-G,SIG,EXP 40-ZR-90(PX)39-Y-85-M,SIG,EXP, 1	11.2 11.2 11.2 11.2
(Birjukov et al., 1979)	$^{91}\text{Zr}$ (63.63 %)	cyclotron single target	beam current integrator	neutron time of flight	40-ZR-90(PN)41-NB-90,SIG, 1	11.2
(Roughton et al., 1979)	$nat$ Zr	cyclotron single target irr.	beam current integrator	$\gamma$ -Ge(Li)	40-ZR-90(PG)41-NB-91-M,PY,TT, 15 40-ZR-94(PN)41-NB-94-M,PY,TT 13 40-ZR-96(PN)41-NB-96,PY,TT, 12	1.75-6.426 3.056-5.953 3.057-5.954
(Muminov et al., 1980)	$nat$ Zr	cyclotron		no chemical separation Ge(Li)	40-ZR-0(PN)41-NB-90-M,TTY, 3	9-11
(Dmitriev and Molin, 1981)	$nat$ Zr	cyclotron single target	Faraday cup	$\gamma$ -Ge(Li)	40-ZR-0(PX)39-Y-88,TTY,DT, 1 40-ZR-0(PX)40-ZR-95,CUM,TTY,DT, 1 40-ZR-0(PX)41-NB-92-M,TTY,DT, 1 40-ZR-96(P2N)41-NB-95-G,TTY,DT, 1	22 22 22 22
(Regnier et al., 1982))	$nat$ Zr	cyclotron linac cyclotron stacked foil	$^{27}\text{Al}(p,x)^{22}\text{Na}$	$\gamma$ -HPGe	40-ZR-0(PX)40-ZR-88,CUM,SIG, 7	59-24000
(Dmitriev, 1983)					40-ZR-92(PN)41-NB-92-M,TTY,EXP, 140-ZR-92(P2N)41-NB-91-M,TTY,EXP, 1 40-ZR-96(P2N)41-NB-95,TTY,EXP, 1 40-ZR-90(PX)40-ZR-89,TTY,EXP, 1 40-ZR-90(PA)39-Y-87,TTY,EXP, 1 40-ZR-96(PX)40-ZR-95,TTY,EXP, 1	22 22 22 22 22
(Abe et al., 1984)	$nat$ Zr	cyclotron multi-sample target method	$^{65}\text{Cu}(p,n)^{65}\text{Zn}$	$\gamma$ -Ge(Li), HPGe	40-ZR-0(PX)41-NB-90-G,M+,TTY,DT, 1 40-ZR-92(PN)41-NB-92-M,TTY,DT, 1 40-ZR-96(PN)41-NB-96,TTY,DT, 1	16 16 16
(Isshiki et al., 1984))	$nat$ Zr	cyclotron rotating target holder	$nat$ Ti(p,x) $^{48}\text{V}$	?-Ge(Li)	40-ZR-0(PN)41-NB-90-M,TTY, 1	10.4
(Batij et al., 1985)	$^{96}\text{Zr}$	LINAC single foil irradiation	Faraday cup	$\gamma$ -Ge(Li)	40-ZR-90(PN)41-NB-90-M,SIG, 4 40-ZR-90(PN)41-NB-90-G,SIG, 3 40-ZR-90(PN)41-NB-90,SIG, 3 40-ZR-92(PN)41-NB-92-M,SIG, 10 40-ZR-96(PN)41-NB-96,SIG, 11	7.5-9 8-9 8-9 4.5-9 4-9
(Konstantinov et al., 1986)	$nat$ Zr	syclotron stacked foil	Faraday cup	$\gamma$ -Ge(Li))	40-ZR-0(PX)39-Y-87-G,TTY,(PHY), 28 40-ZR-0(PX)39-Y-88,TTY,(PHY), 30 40-ZR-0(PX)40-ZR-89-G,TTY,(PHY), 16 40-ZR-0(PX)41-NB-91-M,TTY,(PHY), 18 40-ZR-0(PX)41-NB-92-M,TTY,(PHY), 35 40-ZR-0(PX)41-NB-95-G,TTY,(PHY), 30 40-ZR-0(PX)39-Y-87-G, TTY,(PHY), 1 40-ZR-0(PX)39-Y-88,TTY,(PHY), 1 40-ZR-0(PX)40-ZR-89-G,TTY,(PHY), 1 40-ZR-0(PX)40-ZR-95,TTY,(PHY), 1 40-ZR-0(PX)41-NB-91-M,TTY,(PHY), 1 40-ZR-0(PX)41-NB-92-M,TTY,(PHY), 1 40-ZR-0(PX)41-NB-95-M,TTY,(PHY), 1 40-ZR-0(PX)41-NB-95-G,TTY,(PHY), 1	11-22.4 9.8-22.4 16.8-22.4 15.9-22.4 6.1-22.4 9.8-22.4 22.4 22.4 22.4 22.4 22.4 22.4 22.4 22.4
(Kuzmenko et al., 1987)	$nat$ Zr	cyclotron stacked foil	Faraday cup	$\gamma$ -Ge(Li)	40-ZR-90(PN)41-NB-90-G,SIG, 1 40-ZR-0(PX)40-ZR-89,CUM,SIG, 1 40-ZR-0(PX)39-Y-87,SIG, 1 40-ZR-0(PX)39-Y-86,SIG, 1	17 19 19 28
(Skakun et al., 1987)	$^{90}\text{Zr},^{92}\text{Zr},^{96}\text{Zr}$	LINACsingle foil target	Faraday cup	$\gamma$ -Ge(Li)	40-ZR-90(PN)41-NB-90-M,SIG, 4 40-ZR-90(PN)41-NB-90-G,SIG, 3 40-ZR-90(PN)41-NB-90,SIG, 3 40-ZR-92(PN)41-NB-92-M,SIG,10 40-ZR-96(PN)41-NB-96,SIG, 11	7.5-9 8-9 8-9 4.5-94-9
(Gorpinich et al., 1988)	$nat$ Zr	cyclotron stacked foil	Faraday cup	$\gamma$ -Ge(Li)	40-ZR-0(PX)37-RB-82-M,SIG,EXP, 18 40-ZR-0(PX)37-RB-83, SIG,EXP,24 40-ZR-0(PX)37-RB-84,SIG,EXP, 14	43-9.68 35-68 47.5-68
(Nickles, 1991)	$nat$ Zr	cyclotron	Faraday cup	$\gamma$ -Ge(Li)	40-ZR-90(PN)41-NB-90, TTY, 1 40-ZR-92(PN)41-NB-92-M,TTY, 1 40-ZR-96(PN)41-NB-96,TTY, 1	1111111
(Kondratev et al., 1991)	$nat$ Zr	cyclotron	$^{27}\text{Al}(p,x)^{24}\text{Na}^{nat}\text{Fe}(p,x)^{56}\text{Co}^{nat}\text{Fe}(p,x)^{51}\text{Cr}$	$\gamma$ -Ge(Li)	40-ZR-0(PX)41-NB-90-G,IND/M+,SIG, 39	9.6-68.0
(Vysotsky et al., 1991)	$nat$ Zr	cyclotron stacked foil		$\gamma$ -Ge(Li)	40-ZR-0(PX)39-Y-88,(CUM),SIG,EXP, 640-ZR-0(PX)41-NB-91-M,IND,SIG,EXP, 5 40-ZR-0(PX)41-NB-92-M,SIG,EXP, 5 40-ZR-0(PX)41-NB-95-G,(CUM),SIG,EXP, 6	1.6-5.7 2.8-5.7 2.8-5.7 1.6-5.7
(Levkovskii, 1991)	$^{90}\text{Zr},^{91}\text{Zr},^{92}\text{Zr}$ $^{96}\text{Zr}$	cyclotron rotating target	$nat$ Mo(p,x) $^{96}\text{Tc}$	no chemical separation $\gamma$ -Ge (Li)	40-ZR-90(P2N)41-NB-89-M,SIG, 16 40-ZR-90(Pa)39-Y-87-G,SIG, 13 40-ZR-90(Pa)39-Y-87-M,SIG, 16 40-ZR-90(PN)41-NB-90,SIG, 25 40-ZR-90(PN+a)39-Y-86,SIG, 9 40-ZR-90(PN+a)39-Y-86-M,SIG, 7 40-ZR-90(PX)40-ZR-89,CUM,SIG 40-ZR-90(PN+P)40-ZR-89,SIG+40-ZR-90(P2N)41-NB-89-M,SIG, 20 40-ZR-91(P2N)41-NB-90,SIG, 17 40-ZR-91(Pa)39-Y-88,SIG, 21 40-ZR-91(PN+a)39-Y-87-G,SIG, 8 40-ZR-91(PN+a)39-Y-87-M,SIG, 10 40-ZR-91(PX)40-ZR-89,CUM,SIG 40-ZR-91(P2N+P)40-ZR-89,SIG 40-ZR-91(P3N)41-NB-89-M,SIG, 8 40-ZR-92(P3N)41-NB-90,SIG, 8 40-ZR-92(PN+a)39-Y-88,SIG, 13 40-ZR-96(P2N)41-NB-95-G,SIG, 25 40-ZR-96(P2N)41-NB-95-M,SIG, 25 40-ZR-96(PN)41-NB-96,SIG, 13 40-ZR-96(PN+P)40-ZR-95,SIG, 20	15.8-29.5 18.3-29.5 15.8-29.5 7.7-29.5 22.7-29.5 24-29.5  12.1-29.5 14.8-29.5 9.5-27.6 23.1-29.5 21.4-29.5  23.1-29.5 23.1-29.5 18.3-29.5 7.7-29.5 7.7-29.5 7.7-18.3 12.1-29.5

Table 1: continued

Author	Target	Irradiation	Beam current measurement and monitor reaction	Separation method and measurement of activity	Nuclear reaction and measured quantity and number of measured data points	Covered energy range(MeV)
(Michel et al., 1997)	$^{nat}\text{Zr}$	cyclotron stacked foil	$^{27}\text{Al}(p,x)^{22}\text{Na}$ $^{nat}\text{Cu}(p,x)^{65}\text{Zn}$	no chemical separation $\gamma$ -Ge (Li)	40-ZR-0(PX)41-NB-96.SIG, 23 40-ZR-0(PX)41-NB-95.M.SIG, 38 40-ZR-0(PX)41-NB-95.G.SIG, 52 40-ZR-0(PX)41-NB-91.M.SIG, 39 40-ZR-0(PX)41-NB-90.G.M+.SIG, 72 40-ZR-0(PX)40-ZR-95.CUM.SIG, 69 40-ZR-0(PX)40-ZR-89.CUM.SIG, 91 40-ZR-0(PX)40-ZR-88.CUM.SIG, 85 40-ZR-0(PX)40-ZR-86.CUM.SIG, 30 40-ZR-0(PX)39-Y-88.SIG, 75 40-ZR-0(PX)39-Y-87-M.CUM.SIG, 70 40-ZR-0(PX)39-Y-87-G.CUM/M.SIG, 100 40-ZR-0(PX)39-Y-86.G.M+.SIG, 59	9.48-43.3 9.48-70.1 9.48-2570 9.48-70.1 9.48-2600 9.48-1600 9.48-2600 18.9-2600 54.4-2600 18.9-2570 9.48-156 9.48-2600 22.2-2570
(Busse et al., 2002)	$^{nat}\text{Zr}^{90}\text{ZrO}_2$	cyclotron stacked foil	$^{63}\text{Zn}(p,n)^{63}\text{Zn}$ $^{63}\text{Zn}(p,2n)^{62}\text{Zn}$	no chemical separation $\gamma$ -HPGe	40-ZR-0(PN)41-NB-90.TTY.DT, 5 40-ZR-0(PN)41-NB-90.G.M+.SIG, 16 40-ZR-90(P,2N)41-NB-89.G.SIG, 3 40-ZR-90(P,2N)41-NB-89.M.SIG, 4 40-ZR-90(P,N)41-NB-90.SIG, 12 40-ZR-0(PN)41-NB-90.TTY.DT, 5	8.1-17.6 7.5-15.3 17.8-19.0 17.2-19.0 12.0-19.0 11.9-17.6
(Bringas et al., 2005)	$^{nat}\text{Zr}$	cyclotron stacked foil	$^{63}\text{Zn}(p,2n)^{62}\text{Zn}$ $^{63}\text{Zn}(p,n)^{65}\text{Zn}$	no chemical separation $\gamma$ -HPGe	40-ZR-0(PX)40-ZR-88.CUM.SIG, 2	19.6-27.1
(Uddin et al., 2008)	$^{nat}\text{Zr}$	cyclotron stacked foil	$^{nat}\text{Cu}(p,x)^{62}\text{Zn}$	no chemical separation $\gamma$ -HPGe	40-ZR-0(PX)39-Y-86.SIG, 11 40-ZR-0(PX)39-Y-87.SIG, 15 40-ZR-0(PX)39-Y-87-M.SIG, 12 40-ZR-0(PX)39-Y-88.SIG, 10 40-ZR-0(PX)40-ZR-88.SIG, 9 40-ZR-0(PX)40-ZR-89.SIG, 15 40-ZR-0(PX)41-NB-90.SIG, 15 40-ZR-0(PX)41-NB-92.M.SIG, 15 40-ZR-0(PX)41-NB-95.G.SIG, 11 40-ZR-0(PX)41-NB-96.SIG, 15	18.9-39.7 4.6-39.7 15.1- 39.721.5-39.7 24.6-39.7 4.6-39.7 4.6-39.7 4.6-39.7 6.0-39.7 4.6-39.7
(Khandaker et al., 2009)	$^{nat}\text{Zr}$	cyclotron stacked foil	$^{nat}\text{Cu}(p,x)^{62}\text{Zn}$	no chemical separation $\gamma$ -HPGe	40-ZR-0(PX)41-NB-92.M.SIG, 17 40-ZR-0(PX)41-NB-90.SIG, 16 40-ZR-0(PX)40-ZR-89.G.CUM.SIG, 16 40-ZR-0(PX)40-ZR-88.(CUM).SIG, 8 40-ZR-0(PX)39-Y-87-M.SIG, 14 40-ZR-0(PX)39-Y-86.IND.SIG, 10	1.2-40 5.3-40 5.3-40 28-40 11.7-40 24-40
(Al-Abyad et al., 2012)	$^{nat}\text{Zr}$	cyclotron stacked foil	$^{nat}\text{Cu}(p,x)^{65}\text{Zn}$	no chemical separation $\gamma$ -Ge (Li)	40-ZR-0(PX)41-NB-96.SIG, 13 40-ZR-0(PX)41-NB-95.G.CUM.SIG, 10 40-ZR-0(PX)41-NB-92.M.SIG, 13 40-ZR-0(PX)41-NB-90.SIG, 11 40-ZR-0(PX)39-Y-88.SIG, 8	4.5-16.7 8.7-16.7 4.5-16.7 7.5-16.7 11-16.9
(Naik et al., 2014)	$^{nat}\text{Zr}$	cyclotron stacked foil	$^{nat}\text{Cu}(p,x)^{62}\text{Zn}$	no chemical separation $\gamma$ -HPGe	40-ZR-90(P,2N)41-NB-89-M/G.SIG/RAT, 1 40-ZR-91(P,3N)41-NB-89-M/G.SIG/RAT, 1 40-ZR-92(P,4N)41-NB-89-M/G.SIG/RAT, 6	19.44 22.58 26.6-44.73
(Murakami et al., 2014)	$^{nat}\text{Zr}$	cyclotron stacked foil	$^{nat}\text{Cu}(p,x)^{62}\text{Zn}$	no chemical separation $\gamma$ -HPGe	40-ZR-0(PX)41-NB-96.SIG, 9 40-ZR-0(PX)41-NB-95.M.SIG, 8 40-ZR-0(PX)41-NB-95.G.SIG, 9 40-ZR-0(PX)41-NB-92.M.SIG, 9 40-ZR-0(PX)41-NB-91.M.SIG, 9 40-ZR-0(PX)41-NB-90.G.CUM.SIG, 8 40-ZR-0(PX)40-ZR-95.SIG, 7 40-ZR-0(PX)39-Y-87-G.M+.SIG, 4 40-ZR-0(PX)39-Y-88.SIG, 8	6.4-14.2 8.6-14.2 6.4-14.2 6.4-14.2 6.4-14.2 7.5-14.2 9.5-14.2 12.0-14.2 8.6-14.2
this work	$^{nat}\text{Zr}$	cyclotron stacked foil	$^{27}\text{Al}(p,x)$ $^{nat}\text{Cu}(p,x)^{65}\text{Zn}$ $^{22}\text{Na}$ $^{nat}\text{Cu}(p,x)^{62}\text{Zn}$	no chemical separation $\gamma$ -HPGe	40-ZR-0(PX)41-NB-96.SIG, 19, 40-ZR-0(PX)41-NB-95.M.SIG, 1240-ZR-0(PX)41-NB-95.G.SIG, 31, 40-ZR-0(PX)41-NB-92.M.SIG, 31 40-ZR-0(PX)41-NB-91.M.SIG, 12 40-ZR-0(PX)41-NB-90.G.M+.SIG, 12 40-ZR-0(PX)40-ZR-95.CUM.SIG, 30 40-ZR-0(PX)40-ZR-89.CUM.SIG, 29 40-ZR-0(PX)40-ZR-88.CUM.SIG, 29 40-ZR-0(PX)40-ZR-86.CUM.SIG, 6 40-ZR-0(PX)39-Y-88.SIG, 11 40-ZR-0(PX)39-Y-87-M.CUM.SIG, 30 40-ZR-0(PX)39-Y-87-G.CUM/M.SIG, 30 40-ZR-0(PX)39-Y-86.G.M+.SIG, 28	20.4-69.8 14.7-36.5 14.7-36.5 14.7-69.8 21.8-49.0 14.7-36.5 17.5-69.8 14.7-69.8 19.6-69.8 53.7-69.8 11.7-36.5 17.5-69.8 14.7-69.8 22.3-69.8

SIG-Cross section, TTY-thick target yield, TTD-differential thick target yield, DERIV-derived data, IND-independent formation, CUM-cumulative formation, REL-relative

Table 2: Decay characteristics of the investigated activation products and Q-values of contributing reactions

Nuclide	Decay path	Half-life	$E_{\gamma}$ (keV)	$I_{\gamma}$ (%)	Contributing reaction	Q-value(keV)GS-GS
$^{96}\text{Nb}$	$\beta^-$ : 100 %	23.35 h	460.040 568.871 778.224 810.330 849.929 1091.349 1200.231	26.62 58.0 96.45 11.09 20.45 48.5 19.97	$^{96}\text{Zr}(p,n)$	-620.13
$^{95m}\text{Nb}$	IT: 94.4 % $\beta^-$ : 5.6 % 235.692 keV	3.61 d	235.690	24.8	$^{96}\text{Zr}(p,2n)$	-7513.22
$^{95g}\text{Nb}$	$\beta^-$ : 100 %	34.991 d	765.803	99.808	$^{96}\text{Zr}(p,2n)$	-7513.22
$^{92m}\text{Nb}$	$\epsilon$ : 100 % ( $\beta^+$ : 0.065 %) 135.54 keV	10.15 d	934.44	99.15	$^{92}\text{Zr}(p,n)$ $^{94}\text{Zr}(p,3n)$ $^{96}\text{Zr}(p,5n)$	-2788.23 -17742.15 -32058.5
$^{91m}\text{Nb}$	IT: 96.6 % $\epsilon$ : 3.4 % $\beta^+$ : 0.0013 % 104.605 keV	60.86 d	104.62 1204.67	0.5742.0	$^{91}\text{Zr}(p,n)$ $^{92}\text{Zr}(p,2n)$ $^{94}\text{Zr}(p,4n)$ $^{96}\text{Zr}(p,6n)$	-2039.93 -10674.72 -25628.63 -39944.98
$^{90}\text{Nb}$	$\epsilon$ : 100 % $\beta^+$ : 51.2 %	14.60 h	141.178 1129.224	66.8 92.7	$^{90}\text{Zr}(p,n)$ $^{91}\text{Zr}(p,2n)$ $^{92}\text{Zr}(p,3n)$ $^{94}\text{Zr}(p,5n)$ $^{96}\text{Zr}(p,7n)$	-6893.68 -14087.6 -22722.41 -37676.31 -51992.66
$^{95}\text{Zr}$	$\beta^-$ : 100 %	64.032 d	724.192 756.725	44.2754.38	$^{96}\text{Zr}(p,pn)$ <sup>95</sup> Y decay	-7854.37
$^{89}\text{Zr}$	$\epsilon$ : 100 % $\beta^+$ : 1.53 %	78.41 h	909.15	99.04	$^{90}\text{Zr}(p,pn)$ $^{91}\text{Zr}(p,p2n)$ $^{92}\text{Zr}(p,p3n)$ $^{94}\text{Zr}(p,p5n)$ $^{96}\text{Zr}(p,p7n)$ $^{89}\text{Nb}$ decay	-11968.49 -19162.4 -27797.2 -42751.11 -57067.45
$^{88}\text{Zr}$	$\epsilon$ : 100 %	83.4 d	392.87	97.29	$^{90}\text{Zr}(p,p2n)$ $^{91}\text{Zr}(p,p3n)$ $^{92}\text{Zr}(p,p4n)$ $^{94}\text{Zr}(p,p6n)$ $^{96}\text{Zr}(p,p8n)$ $^{88}\text{Nb}$ decay	-21287.86 -28481.79 -37116.59 -52070.48 -66386.83 -29522.6
$^{86}\text{Zr}$	$\epsilon$ : 100 % $\beta^+$ : 0.05 %	16.5 h	242.8612.0	95.845.8	$^{90}\text{Zr}(p,p4n)$ $^{91}\text{Zr}(p,p5n)$ $^{92}\text{Zr}(p,p6n)$ $^{94}\text{Zr}(p,p8n)$ $^{86}\text{Nb}$ decay	-43090.19 -50284.11 -58918.9 -73872.79 -52708.3
$^{88}\text{Y}$	$\epsilon$ : 100 % $\beta^+$ : 100 %	106.627 d	898.042 1836.063	$\hat{A}$ 93.799.2	$^{90}\text{Zr}(p,2pn)$ $^{91}\text{Zr}(p,2p2n)$ $^{92}\text{Zr}(p,2p3n)$ $^{94}\text{Zr}(p,2p5n)$ $^{96}\text{Zr}(p,2p7n)$	-19835.09 -27029.02 -35663.81 -50617.72 -64934.05
$^{87m}\text{Y}$	$\epsilon$ : 1.57 % $\beta^+$ : 0.75 % IT: 98.43 % 380.82 keV	13.37 h	380.79	78.06	$^{90}\text{Zr}(p,2p2n)$ $^{91}\text{Zr}(p,2p3n)$ $^{92}\text{Zr}(p,2p4n)$ $^{94}\text{Zr}(p,2p6n)$ $^{96}\text{Zr}(p,2p8n)$ $^{87}\text{Zr}$ decay	-29186.82 -36380.74 -45015.54 -59969.44 -74285.77 -33640.98
$^{87g}\text{Y}$	$\epsilon$ : 100 % $\beta^+$ : 0.180 %	79.8 h	388.531 484.805	82.2 89.8	$^{90}\text{Zr}(p,2p2n)$ $^{91}\text{Zr}(p,2p3n)$ $^{92}\text{Zr}(p,2p4n)$ $^{94}\text{Zr}(p,2p6n)$ $^{96}\text{Zr}(p,2p8n)$ $^{87}\text{Zr}$ decay	-29186.82 -36380.74 -45015.54 -59969.44 -74285.77 -33640.98
$^{86}\text{Y}$	$\epsilon$ : 100 % $\beta^+$ : 31.9 %	14.74 h	443.13 627.72 703.33 777.37 1076.63 1153.05 1854.38 1920.72	16.9 32.6 15.4 22.4 82.5 30.5 17.2 20.8	$^{90}\text{Zr}(p,2p3n)$ $^{91}\text{Zr}(p,2p4n)$ $^{92}\text{Zr}(p,2p5n)$ $^{94}\text{Zr}(p,2p7n)$ $^{96}\text{Zr}(p,2p9n)$ $^{86}\text{Zr}$ decay	-40993.3 -48187.2 -56822.0 -71775.9 -86092.2 -43090.19

When complex particles are emitted instead of individual protons and neutrons the Q-values have to be decreased by the respective binding energies of the compound particles: np-d, +2.2 MeV; 2np-t, +8.48 MeV; 2p2n- $\alpha$ , 28.30 MeV. In the case of metastable states a further correction with the level energy in column 1 is also necessary.





Table 5: Activation cross sections of yttrium radioisotopes in proton induced reactions on zirconium

Energy(MeV)	$^{88}\text{Y}$ (mbarn)			$^{87m}\text{Y}$ (mbarn)			$^{87g}\text{Y}$ (mbarn)			$^{86}\text{Y}$ (mbarn)				
<b>VUB ser. 1</b>														
36.5	±	0.3	19.8	±	4.3	8.44	±	0.94	11.8	±	1.3	23.3	±	2.6
35.0	±	0.3	17.0	±	3.7	8.31	±	0.91	11.6	±	1.3	22.7	±	2.5
33.4	±	0.4	16.3	±	3.5	8.01	±	0.89	10.9	±	1.2	21.3	±	2.3
31.8	±	0.4	13.9	±	3.0	7.26	±	0.80	10.7	±	1.2	18.5	±	2.0
30.1	±	0.4	10.0	±	2.2	6.48	±	0.73	9.01	±	1.00	15.8	±	1.7
28.3	±	0.5	6.63	±	1.46	6.43	±	0.73	9.02	±	1.00	13.2	±	1.5
26.4	±	0.5	5.94	±	0.68	6.92	±	0.79	10.4	±	1.2	9.44	±	1.06
24.4	±	0.6	4.56	±	0.50	7.07	±	0.80	11.6	±	1.3	4.39	±	0.52
22.3	±	0.6	3.33	±	0.43	7.84	±	0.88	11.7	±	1.3	0.80	±	0.16
20.0	±	0.7	2.57	±	0.32	5.11	±	0.59	9.76	±	1.09			
17.5	±	0.7	1.89	±	0.26	3.02	±	0.38	5.48	±	0.64			
14.7	±	0.8												
<b>CYRIC, ser. 2</b>														
69.8	±	0.3				203.0	±	22.2	221.8	±	24.0	225.2	±	24.5
66.7	±	0.4				205.9	±	22.5	235.9	±	25.5	180.1	±	19.7
63.9	±	0.4				214.7	±	23.5	248.4	±	26.9	129.1	±	14.2
60.5	±	0.5				211.2	±	23.0	259.9	±	28.1	75.1	±	8.3
57.4	±	0.6				209.6	±	22.8	250.4	±	27.1	73.5	±	8.2
53.7	±	0.7				185.4	±	20.1	224.1	±	24.2	19.3	±	2.2
51.2	±	0.7				153.8	±	16.7	186.6	±	20.2	16.5	±	1.9
49.0	±	0.8				122.2	±	13.4	146.8	±	15.9	14.9	±	1.8
47.2	±	0.8				87.1	±	9.6	108.4	±	11.7	14.8	±	1.8
44.9	±	0.8				52.1	±	5.7	67.5	±	7.3	15.3	±	1.7
43.0	±	0.9				26.0	±	3.4	35.5	±	3.9	17.0	±	2.1
40.5	±	0.9				15.3	±	2.3	19.1	±	2.1	20.2	±	2.4
38.4	±	1.0				10.6	±	2.1	15.5	±	1.7	22.6	±	2.6
35.7	±	1.1				10.7	±	1.9	14.0	±	1.5	25.2	±	2.9
33.2	±	1.1				7.99	±	1.82	12.9	±	1.4	21.3	±	2.5
30.2	±	1.2							11.2	±	1.2	18.8	±	2.2
27.4	±	1.2				4.19	±	1.66	11.3	±	1.2	11.1	±	1.4
23.8	±	1.3				6.84	±	2.43	13.8	±	1.5	2.55	±	0.74
20.4	±	1.4				5.44	±	2.03	11.9	±	1.3			

Table 6: Possible production routes of  $^{90}\text{Nb}$ ,  $^{95}\text{Nb}$ ,  $^{89}\text{Zr}$  and  $^{88}\text{Y}$  radioisotopes at medium energy cyclotrons (Enr. = enriched target material)

Product	Route	Reactions	Energy range	Target	
$^{90}\text{Nb}$	direct	$^{90}\text{Zr}(p,n)^{90}\text{Nb}$	8-20	Enr. $^{90}\text{Zr}$	
		$^{90}\text{Zr}(d,2n)^{90}\text{Nb}$	12-28	Enr. $^{90}\text{Zr}$	
		$^{91}\text{Zr}(p,2n)^{90}\text{Nb}$	20-9	Enr. $^{91}\text{Zr}$	
		$^{89}\text{Y}(\alpha,3n)^{90}\text{Nb}$	30-50	nat Y	
		$^{89}\text{Y}(^3\text{He},2n)^{90}\text{Nb}$	15-25	nat Y	
$^{95m}\text{Nb}$	direct	$^{96}\text{Zr}(p,2n)^{95m}\text{Nb}$	10-25	Enr $^{96}\text{Zr}$	
		$^{94}\text{Zr}(d,n)^{95m}\text{Nb}$	5-15	Enr $^{94}\text{Zr}$	
		$^{96}\text{Zr}(d,3n)^{95m}\text{Nb}$	12-30	Enr $^{96}\text{Zr}$	
$^{89}\text{Zr}$	direct	$^{89}\text{Y}(p,n)^{89}\text{Zr}$	5-20	nat Y	
		$^{89}\text{Y}(d,2n)^{89}\text{Zr}$	10-30	nat Y	
		$^{90}\text{Zr}(p,2n)^{89}\text{Nb}, ^{89}\text{Zr}$	10-25	Enr $^{90}\text{Zr}$	
$^{88}\text{Y}$	direct	nat Sr(p,xn) $^{88}\text{Y}$	5-20	nat Sr	
		nat Sr(d,xn) $^{88}\text{Y}$	5-20	nat Sr	
		nat Rb( $\alpha$ ,xn) $^{88}\text{Y}$	10-20	nat Rb	
		nat Zr(p,x) $^{88}\text{Y}$	30-80	nat Zr	
		indirect	nat Zr(p,x) $^{88}\text{Zr}, ^{88}\text{Y}$	30-80	nat Zr
		$^{89}\text{Y}(p,x)^{88}\text{Nb}, ^{88}\text{Zr}, ^{88}\text{Y}$	15-35	nat Y	